International Journal of Microwave and Wireless Technologies

cambridge.org/mrf

A dipole-coupled metal-mountable UHF RFID antenna based on a vertical loop structure

Xueliang Yang[1], Fei He[1,2], Peng Wang[1], Kaichao Wang[1], Yuanjian Liu[1], Zhenzhen Tu[3] and Weigang Wang[1]

[1]College of Electronic and Optical Engineering & College of Flexible Electronics (Future Technology), Nanjing University of Posts and Telecommunications, Nanjing, China; [2]China Unicom Data Technology Co., Ltd., Nanjing, China and [3]School of Materials Science & Engineering, Nanjing University of Posts and Telecommunications, Nanjing, China

Research Paper

Cite this article: Yang X, He F, Wang P, Wang K, Liu Y, Tu Z, Wang W (2026) A dipole-coupled metal-mountable UHF RFID antenna based on a vertical loop structure. *International Journal of Microwave and Wireless Technologies* **18**(2), 222–234. https://doi.org/10.1017/S1759078726103249

Received: 29 December 2025
Revised: 7 April 2026
Accepted: 13 April 2026

Keywords
tag; UHF; metal-mount

Corresponding author: Weigang Wang; Email: wangwg2020@163.com

Abstract

This paper presents a novel UHF RFID tag antenna with metal-mount capability, broadband characteristics, and frequency controllability. To achieve anti-metal performance, we explore a vertical loop structure as the main radiator, with slots for frequency adjustment and layout flexibility. The antenna operates based on a hybrid magnetic–electric mode interaction mechanism, in which the vertical loop provides a magnetic-dipole-dominated radiation mode. Furthermore, asymmetric resonant dipole patches are loaded on both sides of the center feed line to introduce an auxiliary electric mode and broaden the operating bandwidth. This structural-level mode and coupling engineering enables independent control of the center frequency while maintaining wideband impedance matching. The proposed antenna has a compact size of $0.1951\lambda \times 0.128\lambda \times 0.0051\lambda$, with the main radiation lobe concentrated within 60° from the zenith. By mounting on a 100 × 100 × 2 mm^3 copper plate, it achieves a maximum read range of 7.32 m, which demonstrates the good adaptability for UHF RFID tagging on metal surfaces.

Introduction

UHF tag antennas offer a long reading distance for RFID systems. As a result, UHF RFID systems have attracted much attention in recent years [1]. The key factors determining long read ranges include tag antenna gain, power transmission coefficient, and RFID chip sensitivity [2, 3]. Owing to their long read range, fast identification, and low cost, passive UHF RFID tags are now mainstream in global commercial and industrial systems [4, 5]. However, when a UHF RFID tag is placed on a metal surface or other high-permittivity materials, its impedance matching and radiation performance degrade greatly because of metal reflection and strong coupling. This causes a shift in the operating frequency and a sharp drop in reading distance [6, 7].

To solve these problems, researchers have proposed various metal-mountable tag design methods, including the use of artificial magnetic conductors, electromagnetic tape gap structures, defected ground structures, and parasitic elements to improve radiation performance in metallic environments [8–10]. Among them, the magnetic loop antenna can reduce the interference from metal because of its special field distribution. It also has a symmetric structure and can fit well on the tag substrate. Therefore, it has become an important direction for designing anti-metal RFID tags [11, 12]. Magnetic loop antennas reduce the impact of induced eddy currents on metallic surfaces on antenna performance through closed magnetic fields formed by loop currents. However, a single magnetic loop structure still has limitations in impedance matching flexibility and bandwidth expansion, which makes it difficult to fully meet the requirements of complex industrial scenarios [13].

In practical applications, UHF RFID tags often need to cover a wide operating frequency band to adapt to frequency allocations in different countries or regions (902–928 MHz in North America, 865–868 MHz in Europe, and 920–925 MHz in China) [14]. Although a traditional single-resonant vertical loop antenna has good potential for anti-metal performance, its inherent bandwidth is narrow and cannot cover multiple bands at the same time. It also needs an extra and complex matching network to match the input impedance of the RFID chip, which increases structural complexity and loss [15]. To meet this demand, recent studies have attempted to achieve bandwidth expansion and impedance optimization using methods such as multi-resonance structures, parasitic element coupling, and composite radiator combinations [16, 17]. Reference [11] proposed a compact vertical magnetic loop antenna that achieves omnidirectional radiation through magnetic loop conductors and enhances metal-mountable performance using loop magnetic fields. However, the antenna has a narrow bandwidth and its size was limited by the loop diameter. Subsequently, in [18], researchers applied fractal geometry to the vertical loop and proposed a polygonal fractal loop antenna. By iteratively expanding

© The Author(s), 2026. Published by Cambridge University Press in association with The European Microwave Association.

the loop area, the induced voltage and radiation performance are effectively enhanced, thereby improving read range and gain. This design showed more stable resonance on different materials, but the bandwidth was still relatively limited. Then, in [19], the literature proposed a microstrip collinear loop array antenna, which achieved in-phase current distribution to generate a uniform magnetic field by introducing periodic radiation elements into the loop structure. The array formed a significantly amplified reading/writing area in the near-field and achieved omnidirectional radiation in the far-field. Through the superposition of loop array structures, wider impedance bandwidth and higher gain are obtained, significantly improving the read performance of traditional single-loop antennas. Finally, in [12], a ring-coupled folded patch antenna was proposed. By adding narrow shorted branches to the folded patch, adjacent resonances were formed in the original vertical loop structure. It provided a simple and low-cost wideband anti-metal design. This method did not require extra stacked layers. The bandwidth could be tuned simply by adjusting the branch width and the antenna could achieve long reading distance across the entire UHF RFID band in North America.

Based on the above background, we propose a UHF RFID tag antenna combining a magnetic loop antenna with dipoles. By placing the magnetic loop antenna on a metal surface, the part in contact with the metal isolates the top patch from the metal [20] and thus endows the antenna anti-metal performance. In addition, to compensate for the low gain and narrow bandwidth of the vertical loop, we design the high radiation efficiency and easy impedance matching of a dipole structure. Dipole radiating arms are thus loaded on both sides of the tag chip's feed line [21, 22]. A dual-resonant characteristic is created by coupling between the feed line and the dipoles. By adjusting the dipole lengths, their resonant frequencies are tuned to lie above and below the target frequency of 915 MHz. This achieves broad frequency band coverage. The proposed antenna features a compact structure, low profile, ease of fabrication, and broadband anti-metal performance. All in all, it is suitable for managing metal assets and logistics tracking in industrial environments.

The main contributions of this work are summarized as follows:

1. A vertical magnetic loop–electric dipole hybrid radiator is proposed, which enables a dual-mode radiation mechanism suitable for on-metal RFID tags.
2. A dual-resonant coupling scheme based on asymmetric dipoles is introduced to achieve broadband impedance matching without stacked substrates or lumped components.
3. The proposed structure exhibits enhanced frequency stability on metallic surfaces, attributed to the complementary frequency-shift behavior of magnetic and electric modes.

Antenna structure design and operating principle

Basic antenna structure

The structural configuration of the proposed antenna is shown in Figure 1. Fabricated via standard PCB etching technology, the antenna employs a 0.035 mm-thick copper radiator and a 1.6 mm-thick FR4 substrate with a dielectric constant of 4.4. This design incorporates a magnetic loop structure. The tag chip is placed at the center of the loop's feed line. The distance from the chip to each end patch is $L1$. Slots with dimensions length (a) and width (b) are cut into two end patches. Asymmetric dipole structures are positioned on both sides of the feed line, with their dimensions defined by $L2$, $W2$ and $L3$, $W3$. The length and width of these dipole arms

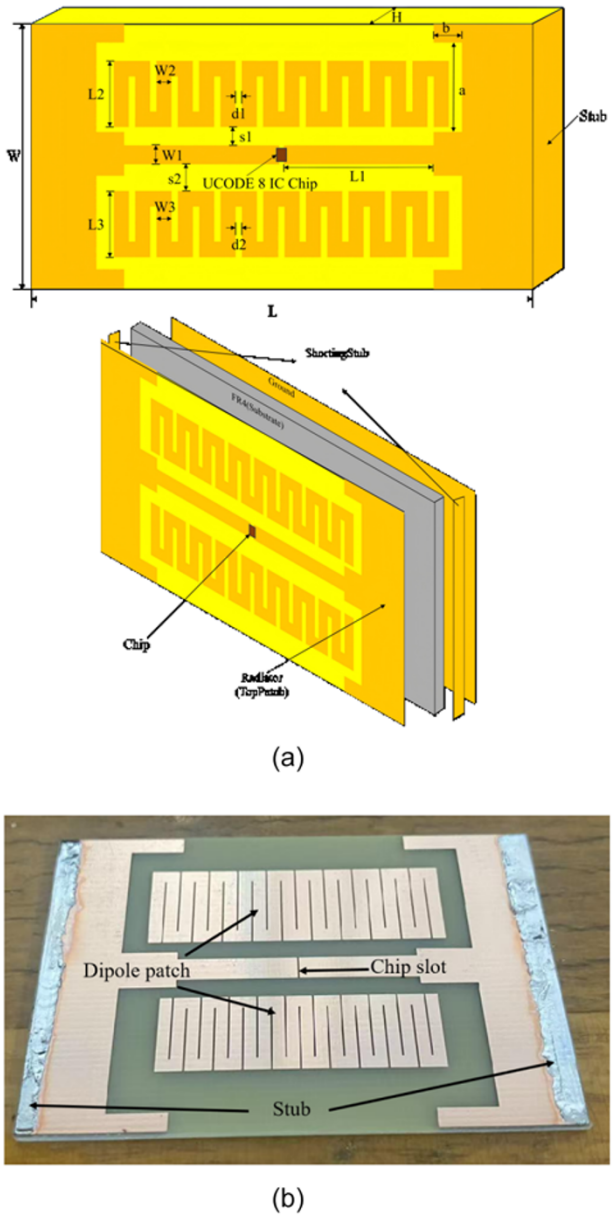


Figure 1. Structure of tag antenna. (a) Tag antenna structure configuration. (b) Prototype physical image.

decides the antenna's impedance matching. The RFID IC matched with the antenna in this design is UCODE 8, bonded across a narrow gap. The microchip has a read sensitivity of −21.85 dBm and an impedance of $13–j191\Omega$ at 916 MHz.

We design and optimize the tag antenna, and study its input impedance, radiation efficiency, and gain in Ansys HFSS. The design dimensions are summarized in Table 1.

Although the overall layout may appear relatively large compared with some compact RFID tags, its physical dimensions correspond to $0.1951\lambda \times 0.128\lambda \times 0.0051\lambda$ at 915 MHz. From an electrical perspective, the antenna remains electrically small in thickness and moderate in aperture size.

In metal-mount RFID applications, a certain ground clearance and loop aperture are necessary to maintain stable magnetic radiation. Excessive miniaturization often leads to degraded radiation efficiency and reduced read range. Therefore, the proposed

https://doi.org/10.1017/S1759078726103249 Published online by Cambridge University Press

Table 1. Dimensions of the antenna

Parameter	Value (mm)	Parameter	Value (mm)
L	64	W3	1.7
W	42	a	16
H	1.6	b	7
L1	15	d1	0.2
L2	9.6	d2	0.2
L3	11.2	s1	4
W1	1	s2	4
W2	1.5		

size represents a trade-off between compactness and radiation performance.

Structurally, the antenna consists of two clearly defined functional parts. The vertical loop acts as the primary magnetic radiator and ensures metal tolerance. The asymmetric meandered dipole branches are not independent radiators. They serve as auxiliary resonators for impedance tuning and bandwidth control. The entire structure remains planar and adopts a simple double-layer configuration without vias or multilayer stacking, which keeps fabrication complexity low.

Design procedure

The fundamental reason for the performance degradation of UHF RFID tags in metallic surface applications lies in the image effect caused by metallic conductors [5, 8]. When placed parallel to metal, an antenna's operation is disrupted by the induced image current. Because this image current is out-of-phase with the source current, their combined fields cancel each other out. This leads to strong radiation cancellation and impedance detuning, which ultimately cause a severe reduction or complete loss of read range [11, 18].

To overcome this difficulty, we did not adopt the traditional dipole parallel to the metal surface. Instead, we introduce a vertical loop structure placed perpendicularly to the metal as the core solution for metal-mount capability. The rationale and advantages of this design are detailed below.

First, the magnetic loop structure can be interpreted as a mirror-type antenna system. When its center feed is connected to the metal ground plane via a shorting pin, the loop arms and the metal surface together form the radiator [23]. Thus, the metal surface is transformed from a disruptive element into an integral artificial ground plane of the antenna system. The image currents on the metal are in-phase with the real currents, which contribute to cooperative radiation that significantly enhances the forward gain [24, 25].

Second, this structure effectively suppresses surface wave loss. The main radiator is elevated away from the metal surface, concentrating its major electric field components in free space rather than in the lossy medium. This prevents energy from being absorbed or trapped by the metal, which greatly improves the radiation efficiency [26, 27].

As shown in Figure 2(a), both ends of the feed line are connected to the backside by a shorting stub. A slot of length (a) and width (b) is etched near each stub to adjust impedance and accommodate the subsequent integration of asymmetric dipoles. To simulate

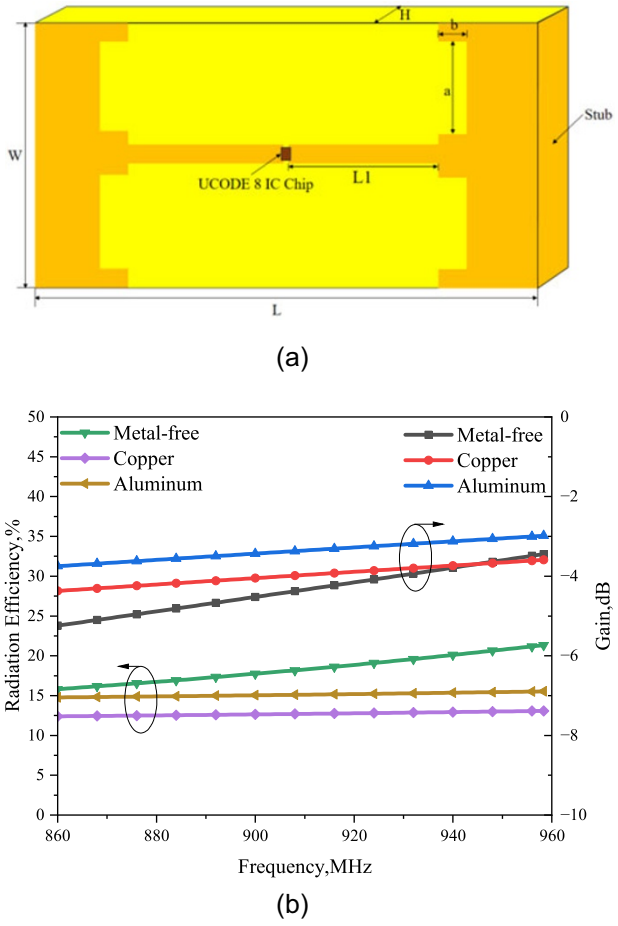


Figure 2. Radiation efficiency and gain on different metallic surfaces. (a) Structure configuration. (b) Radiation efficiency and gain.

performance on metal, $100\times100\times2\,\text{mm}^3$ metal plates of different materials were placed beneath the antenna. Figure 2(b) shows the radiation efficiency and gain when placed on metal plates of different materials. It can be seen that this antenna structure has good metal-mountable interference characteristics.

The current distribution on the antenna was simulated to illustrate its anti-metal operating mechanism. For clarity, the underlying copper plate is hidden in Figure 3. At the 0° phase, the flow of the strongly resonant loop current along the vertical ring structure is clearly visible. This loop current exhibits a uniform, in-phase distribution, indicating a radiation pattern dominated by an effective magnetic dipole. The magnetic field generated by this current path is less affected by the metal in the near-field region. This mechanism avoids the performance degradation seen in electric dipoles, whose electric field is short-circuited by the metal. Consequently, this novel magnetic loop structure effectively improves radiation efficiency on metal surfaces.

The corresponding input impedance, gain, and radiation efficiency on the copper plate are shown in Figure 4. The results show that a gain of −3.92 dBi and a radiation efficiency of 12.74% can be maintained despite the metal presence. However, the input impedance is severely mismatched with the tag chip.

Although the vertical loop structure ensures stable radiation and metal-mount capability, the results in Figure 4 show severe impedance mismatch with the highly capacitive RFID chip. This

https://doi.org/10.1017/S1759078726103249 Published online by Cambridge University Press

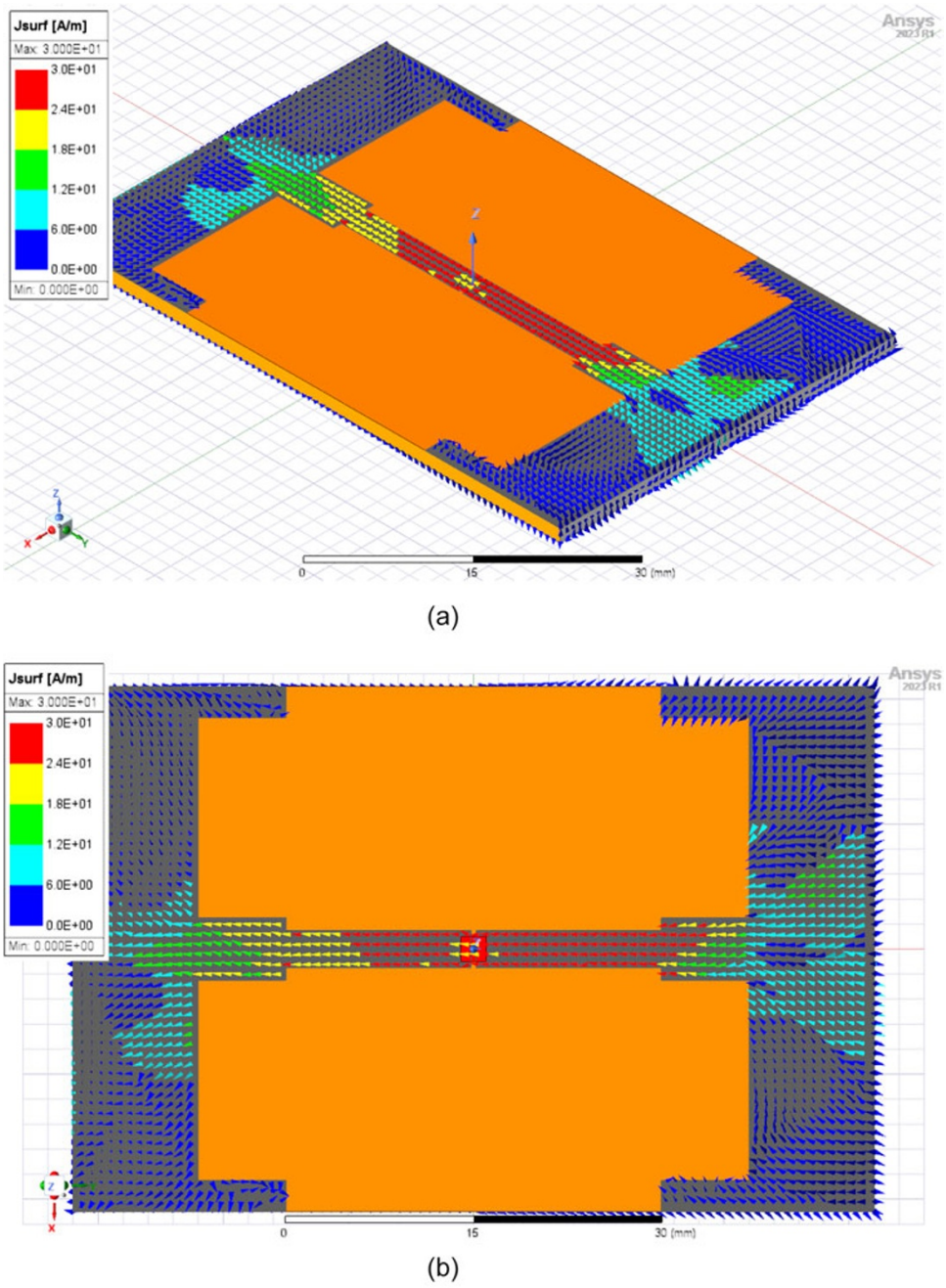


Figure 3. Surface current distribution of the magnetic loop structure. (a) Isometric view. (b) Top view.

is mainly attributed to the inherently single magnetic resonance of the loop, which indicates the necessity of introducing an additional controllable resonant mode.

The proposed antenna operates based on a hybrid magnetic–electric mode interaction mechanism, which fundamentally distinguishes it from conventional single-mode metal-mountable RFID tag antennas.

When the vertical loop structure is placed perpendicular to a metallic surface, the dominant radiation mechanism is governed by a magnetic dipole mode. The loop current forms a closed path normal to the metal plane, generating a magnetic field that satisfies the boundary condition $B_{\perp} = 0$ on a perfect conductor. As a result, the image current induced on the metal surface is in phase with the original loop current, which leads to constructive radiation rather than cancellation. This mechanism enables the vertical loop to maintain stable radiation performance in close proximity to metal.

However, a pure magnetic loop radiator typically exhibits a high quality factor (Q) and limited impedance tuning freedom. This characteristic restricts the achievable bandwidth and complicates conjugate matching with highly capacitive RFID chips.

To address this limitation, asymmetric bent dipole branches are introduced on both sides of the inductive feed line. These dipole branches primarily support an electric dipole mode, which is excited through near-field electromagnetic coupling rather than direct feeding.

https://doi.org/10.1017/S1759078726103249 Published online by Cambridge University Press

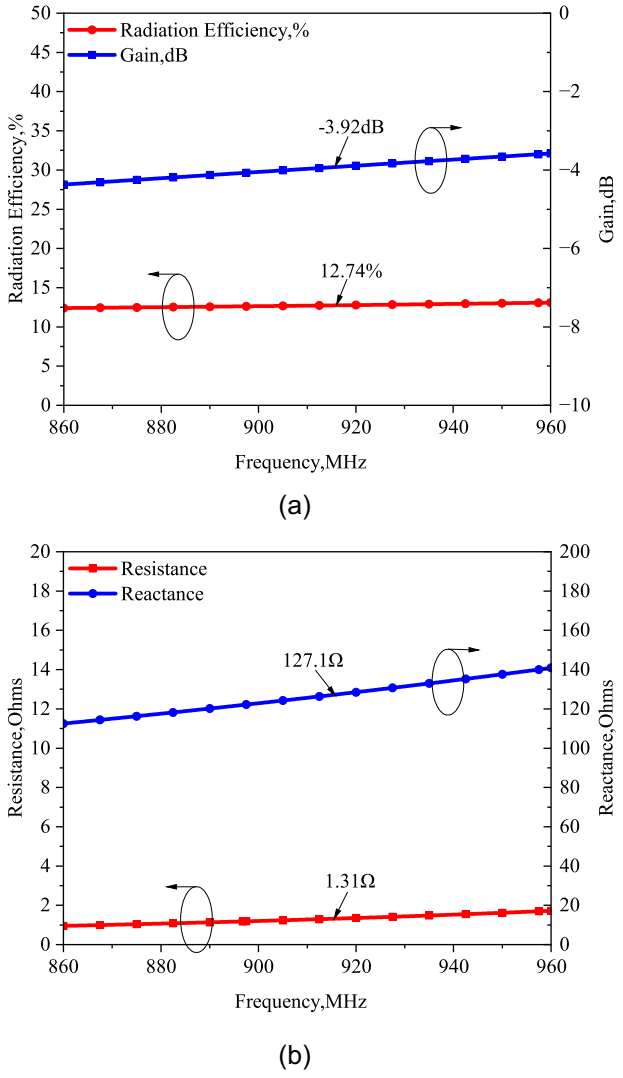


Figure 4. (a) Radiation efficiency and gain. (b) The resistance and reactance of antenna.

The coexistence of magnetic and electric modes results in a dual-mode resonance behavior. The magnetic loop serves as the dominant radiator, ensuring metal-mount capability and radiation stability, while the electric dipole branches act as auxiliary resonators that introduce additional reactive paths. This interaction effectively reduces the overall radiation Q-factor and reshapes the input impedance trajectory, enabling broadband impedance matching without the need for lumped elements or multilayer structures.

More importantly, the two modes exhibit complementary frequency-shift tendencies in metallic environments. The resonance associated with the magnetic loop tends to shift upward due to reduced effective inductance near the metal surface, whereas the electric dipole resonance shifts downward owing to increased capacitive coupling. When properly designed, these opposite tendencies partially compensate for each other, resulting in enhanced resonance stability under metal loading.

Therefore, the proposed antenna does not rely on material engineering or artificial ground structures to achieve metal tolerance. Instead, it realizes broadband and stable on-metal performance through mode engineering at the structural level, by deliberately coupling magnetic and electric resonances within a compact single-layer configuration.

In RFID systems, the read range is a key performance metric. It defines the maximum distance at which a reader can reliably detect a tag's backscattered signal. For passive UHF RFID systems, the maximum read range is mainly limited by the tag's activation distance because the sensitivity of reader antenna is much higher. The maximum read range of a tag can be calculated using the Friis free-space transmission formula

$$R_{tag} = \frac{\lambda}{4\pi}\sqrt{\frac{P_t G_t G_r \tau}{P_{th}}}, \tag{1}$$

where P_t is the transmit power of the reader antenna. G_t is the gain of the reader antenna, and P_{th} is the read sensitivity of the tag chip. G_r is the gain of the tag antenna, and τ is the power transmission coefficient. τ can be calculated by

$$\tau = \frac{4R_A R_L}{|Z_A + Z_L|^2}, \tag{2}$$

where R_A is the antenna resistance, and Z_A is the antenna reactance. R_L is the load resistance, and Z_L is the load reactance [8, 14, 18].

Therefore, impedance matching is a crucial step in designing UHF RFID tag antennas. It is difficult to achieve impedance matching by using only a magnetic loop structure, and its equivalent input impedance exhibits a typical series resonance response. Z_{in} is calculated by

$$Z_{\text{in}} = R + j(\omega L - \frac{1}{\omega C}). \tag{3}$$

The dual-resonant design is inspired by gap-coupled patch technology, which enhances bandwidth performance by coupling two patches with different resonant frequencies to the same loop [17]. Accordingly, asymmetric dipole structures are added on both sides of the feed line. Their flexible impedance characteristics enable precise conjugate matching with the tag chip. Its theoretical basis can be described by a dual-resonance equivalent circuit model and Z_{in} can be calculated by

$$Z_{\text{in}} = R_1 + j(\omega L_1 - \frac{1}{\omega C_1}) + \frac{j\omega M^2}{R_2 + j(\omega L_2 - \frac{1}{\omega C_2})}, \tag{4}$$

where M is the mutual inductance coefficient between the loop feed line and the dipole arms.

To provide further physical insight into the proposed dual-resonant behavior, the antenna is interpreted using classical transmission-line and mutual coupling theory.

The vertical loop structure operates as a small-loop radiator whose circumference is electrically small compared with the operating wavelength. According to small-loop antenna theory, the loop mainly stores magnetic energy and can therefore be modeled as an inductive element. Its input impedance is obtained by

$$Z_{\text{loop}} = R_1 + j\omega L_1, \tag{5}$$

where R_1 represents the radiation and ohmic losses, and L_1 denotes the equivalent inductance of the loop.

The meandered dipole branches located on both sides of the feeding strip behave as electrically lengthened dipole resonators. Each branch can be described using transmission-line theory as a terminated transmission-line section. The input impedance of the dipole branch is given by

https://doi.org/10.1017/S1759078726103249 Published online by Cambridge University Press

$$Z_{\text{dipole}} = -jZ_0 \cot(\beta l_d), \tag{6}$$

where Z_0 is the characteristic impedance, β is the phase constant, and l_d denotes the effective electrical length.

Since the dipole branches are not directly connected to the feeding port, energy transfer occurs through magnetic coupling between the loop current and the dipole currents. Based on mutual inductance theory, the induced voltage generated in the dipole branch produces a reflected impedance at the loop port, expressed as

$$Z_{\text{ref}} = \frac{(j\omega M)^2}{Z_{\text{dipole}}}, \tag{7}$$

where M denotes the mutual inductance between the loop and the dipole branches.

Accordingly, the overall equivalent impedance is obtained by

$$Z_{\text{in}} = Z_{\text{loop}} + Z_{\text{ref}} = R_1 + j\omega L_1 + \frac{(j\omega M)^2}{Z_{\text{dipole}}}. \tag{8}$$

Figures 5 and 6 depict the effects of the dipole patch length ($L2$) and the spacing between the dipole patch and the feed line ($s1$) on the input impedance in a single-resonance antenna, with parameter $L2$ adjusted from 9 to 13.8 mm and parameter $s1$ adjusted from 2.4 to 4.8 mm. In these figures, it can be seen that the resonance frequency of the antenna decreases with the increase of $L2$ and $s1$, which indicates that $L2$ and $s1$ are effective parameters for coarse-tuning the resonance frequency.

Embedding efficient dipole radiators into the loop structure will enhance the overall radiation efficiency and gain. Figure 7 compares the radiation efficiency and gain of the magnetic loop structure without a patch, a single coupled patch, and double patches. Figure 8 shows the maximum simulated realized gain for different configurations. Obviously, the dual-coupled antenna achieves higher radiation efficiency and gain than the single-coupled and basic loop designs under the same parameters. Therefore, the dual-coupled antenna was selected for our optimization.

The coupling between the feed line and the patches allows us to adjust parameters $L2$ and $s1$ to tune the input impedance. We found two sets of parameters for the coupled patches, which create resonances below and above 915 MHz. Figure 9 shows the reflection coefficient (S11) of the proposed tag antenna under both single-resonant and dual-resonant conditions. Due to the complex nature of the chip impedance, S11 is calculated by

$$S_{11} = \frac{Z_{\text{in}} - Z_0^*}{Z_{\text{in}} + Z_0}, \tag{9}$$

where Z_{in} is the antenna impedance and Z_0 is the chip impedance. Figure 9 shows the return loss diagrams of single-resonance patches placed on the upper and lower layers of the feed line and dual-resonance patches. Dual-resonance occurs when both patches are coupled to the loop simultaneously. The results confirm that this modification effectively enhances the bandwidth and achieves optimized impedance matching.

Although the operating bandwidth is broadened, the antenna still exhibits a relatively narrow impedance bandwidth in the lower frequency region, which is mainly determined by the magnetic loop resonance. In practical UHF RFID applications, region-specific frequency allocations do not require ultra-wide bandwidth. A stable resonance improves matching reliability and read consistency on metal surfaces.

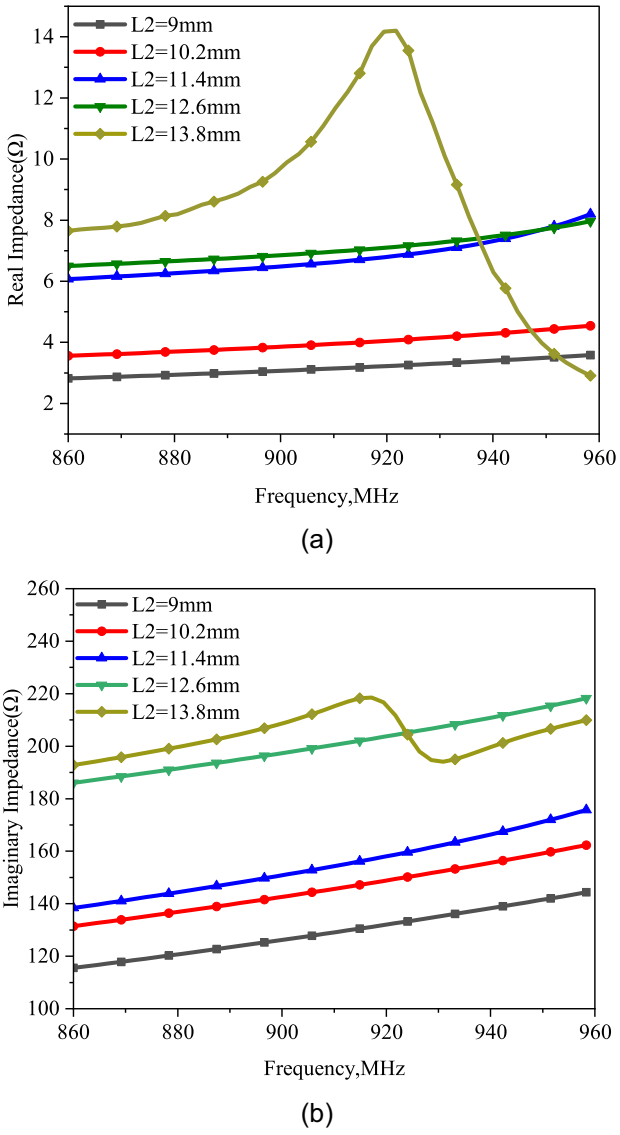


Figure 5. (a) The real impedance varying with $L2$. (b) The imaginary impedance varying with $L2$.

From an application perspective, the proposed structure provides a balanced trade-off among compact size, mechanical simplicity, impedance controllability, and metal tolerance. The antenna maintains stable read range performance while avoiding complex multilayer or via-based structures. These characteristics make it suitable for industrial metal-tagging scenarios where robustness and cost efficiency are critical.

The current distribution of the dual-resonant antenna is shown in Figure 10. It can be seen that the surface currents are not confined to the feeding region but are effectively coupled to the two meandered dipole branches located on both sides of the vertical loop. The currents propagate continuously along the folded paths, which demonstrates that the meandered sections actively participate in resonance rather than acting as parasitic metallic parts.

The folded geometry increases the effective current path without enlarging the physical size, thereby extending the electrical length and enabling low-frequency resonance. Moreover, noticeable current intensity is maintained along the meandered arms,

https://doi.org/10.1017/S1759078726103249 Published online by Cambridge University Press

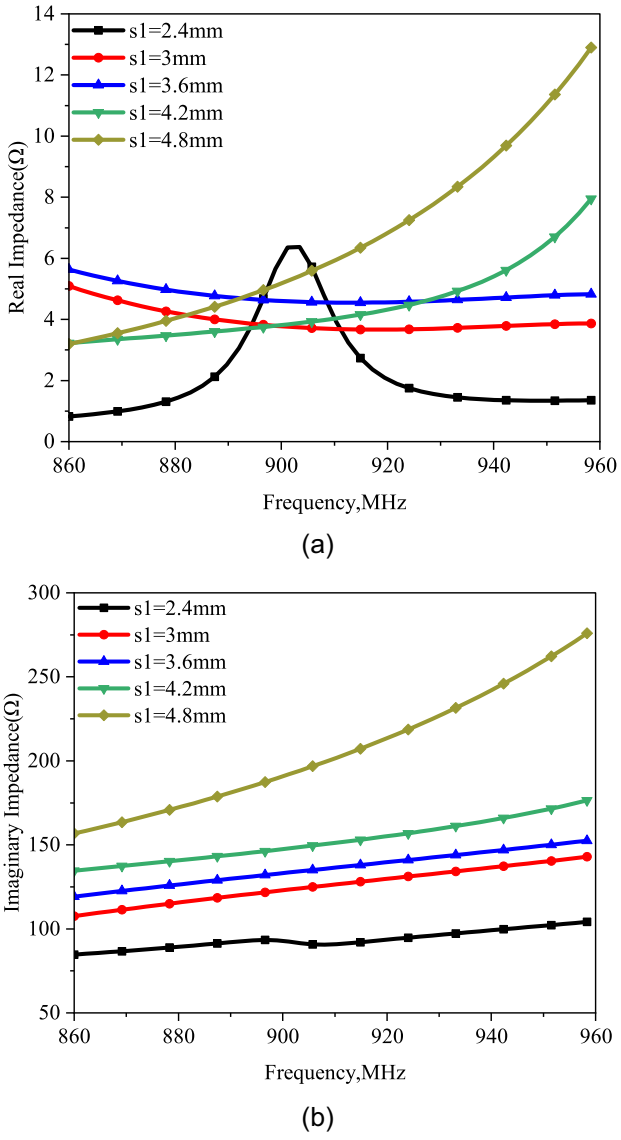


Figure 6. (a) The real impedance varying with *s*1. (b) The imaginary impedance varying with *s*1.

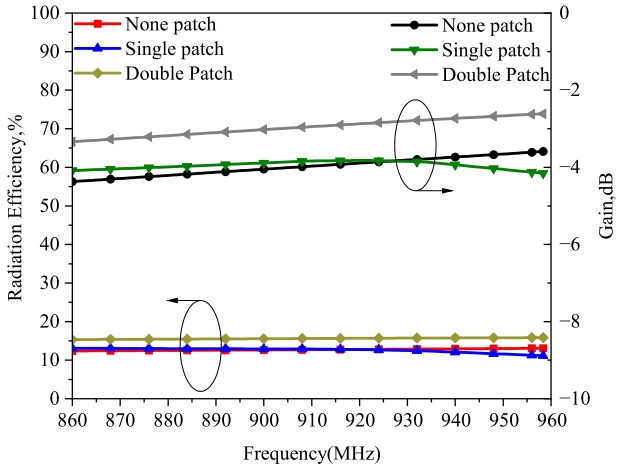


Figure 7. Radiation efficiency and gain for different antennas.

which indicates strong magnetic coupling between the vertical loop and the dipole branches. The induced currents generated through this coupling enhance the overall current magnitude and contribute to the formation of an additional resonant mode.

Therefore, the surface current distributions verify that the coupled meandered dipoles simultaneously realize electrical-length extension and current enhancement, which together lead to the proposed dual-resonant operation.

Furthermore, our antenna achieves active and controllable tuning of the center frequency through its structural parameters. By adjusting the dimensions of the asymmetric dipoles on both sides of the feed line, the shift in resonant frequency can be precisely controlled. Slots (length *a*, width *b*) are etched beside the resonant patches to meet different regional UHF band requirements. The center frequency of the tag antenna is effectively adjusted by varying the length of the asymmetric dipoles (*L*2, *L*3), as shown in Figure 11.

Results and discussion

Impedance matching and radiation characteristics

Based on the design parameters provided in Table 1, the proposed tag antenna was simulated, fabricated, and measured sequentially. We adopted the dual-port S-parameter method to measure the input impedance, which is based on the principle of assuming the existence of a virtual metallic ground at the antenna's symmetric center. Under this premise, the driving voltage can be decomposed into two components (V1 and V2), which are not affected by the distributed current of the antenna. The right arm of the dipole antenna and the virtual ground are regarded as Port 1, and the left arm and the virtual ground are regarded as Port 2. By measuring the S-matrix of this two-port network, all terms of the impedance Z-matrix can be obtained. S_{11}, S_{12}, S_{21}, and S_{22} are measured, where Z_0 is the characteristic impedance of the semi-rigid coaxial cable used to fabricate the test fixture (50 Ω) [17, 21]. Z_d can be calculated by

$$Z_d = \frac{2Z_0(1 - S_{11}S_{22} + S_{12}S_{21} - S_{12} - S_{21})}{(1 - S_{11})(1 - S_{22}) - S_{21}S_{22}} \tag{10}$$

As shown in Figure 12, the antenna was tested in free space and mounted on a $100 \times 100 \times 2$ mm^3 copper plate to simulate real-world metal deployment. A test fixture was made by soldering the outer conductors of two semi-rigid coaxial cables together. The fixture was connected to a Vector Network Analyzer. Port extension was applied to move the calibration reference plane to the ends of the fixture. Finally, the tag antenna under test was connected to the fixture. The antenna's input impedance was calculated from the measured two-port S-parameters using Equation (4).

The measured data were substituted into Equation (4) to obtain the impedance diagram shown in Figure 13. It can be seen that even with certain errors, the antenna still maintains good impedance characteristics when closely attached to the metal plate.

The measured impedance calculated from Figure 13(b) was substituted into Equation (9) to derive the measured S11; the simulated and measured S11 were shown in Figure 14.

The simulated radiation pattern of the tag antenna at 915 MHz is shown in Figure 15. As shown by the radiation distribution in the *xy*-plane in Figure 15(a), the gain in the radiation pattern remains above −7 dB at $\theta = 60°$, and it can even exceed −4 dB at $\theta = 45°$. The radiation distributions in the *xz*-plane and *yz*-plane are shown

https://doi.org/10.1017/S1759078726103249 Published online by Cambridge University Press

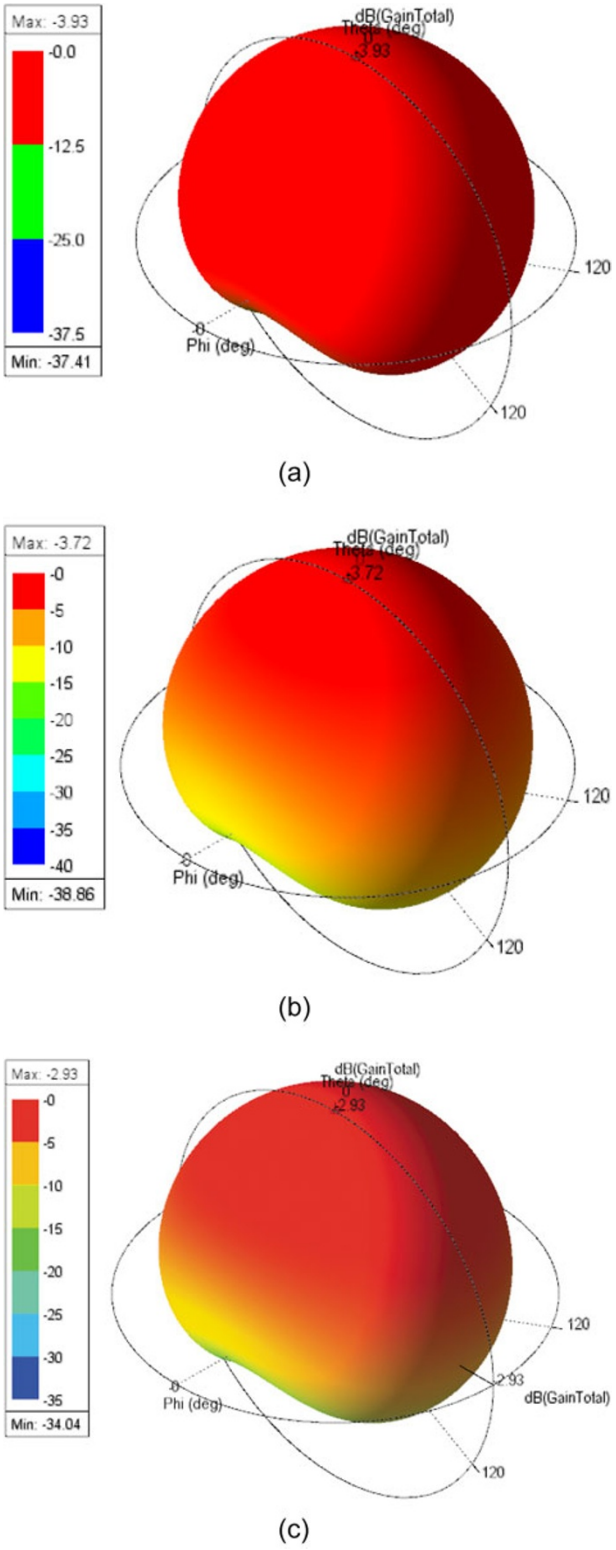


Figure 8. Maximum simulated realized gain of the antenna. (a) None-patch. (b) Single-patch. (c) Double-patch antennas.

in Figure 15(b). It shows that the main radiation coverage of this antenna is within these regions, which exhibits a sectorial radiation characteristic.

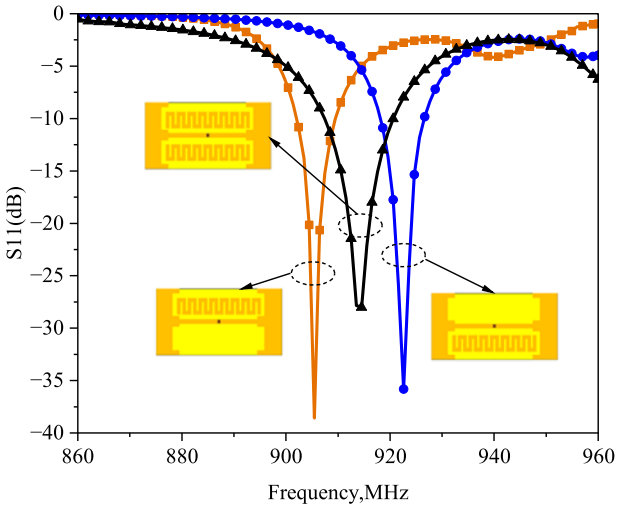


Figure 9. Reflection coefficient of the antenna in single-resonant and dual-resonant modes.

Read range

The tag was evaluated in an anechoic chamber, as shown in Figure 16. The realized gains of the proposed tag antenna for both simulation and measurement were compared in Figure 17. Referring to the same figure, the measured realized gain is −3.12 dBi at 0.910 GHz, which differs slightly from the simulated counterpart, −2.93 dBi at 0.915 GHz. The insignificant difference could be due to imperfection in the fabrication processes.

Then we measured the read range of the tag. The tag antenna was fixed first. Then we kept moving the reader antenna until the backscattered signal from the tag antenna was lost. The measured read range was 6.7 meters without a metal ground plane and 7.3 meters with it, which confirmed excellent metal-mount capability and practicality.

Comparison

As summarized in Table 2, the performance of the proposed antenna was compared against several existing metal-mounted UHF RFID tag designs. The stub-loaded dipole proposed in [8] was low-profile and achieved a read range of 9.75 m in the NA band by adopting a low-cost PTFE substrate. However, it could only switch between the NA and LEu dual bands and did not support wideband operation. In [10], a patch-loaded loop antenna covered both LEu and NA bands by using a single-layer substrate, and it yielded an 8–9 m read range on metal containers. However, its performance was highly sensitive to layer alignment, with a 0.5 mm patch misalignment, which leads to impedance mismatch. The complementary coupled C-patch antenna presented in [14] attained wideband tuning from 920 MHz to 1.18 GHz and a read range of 9 m without relying on lumped components. However, it had drawbacks such as a large size, an inflexible foam substrate, and significant sensitivity to chip placement. The asymmetric SRR antenna in [15] supported independent LEu/NA tuning with a compact structure and achieved a read range of 5 m on a 20×20 cm metal plate. Yet, it required precise positioning of shorting pins to excite even/odd modes, as an offset of 0.5 mm caused a frequency detuning of over 5 MHz, and it exhibited low radiation efficiency, which was only 3–3.25%. [16] introduced a shorted C-patch antenna that

https://doi.org/10.1017/S1759078726103249 Published online by Cambridge University Press

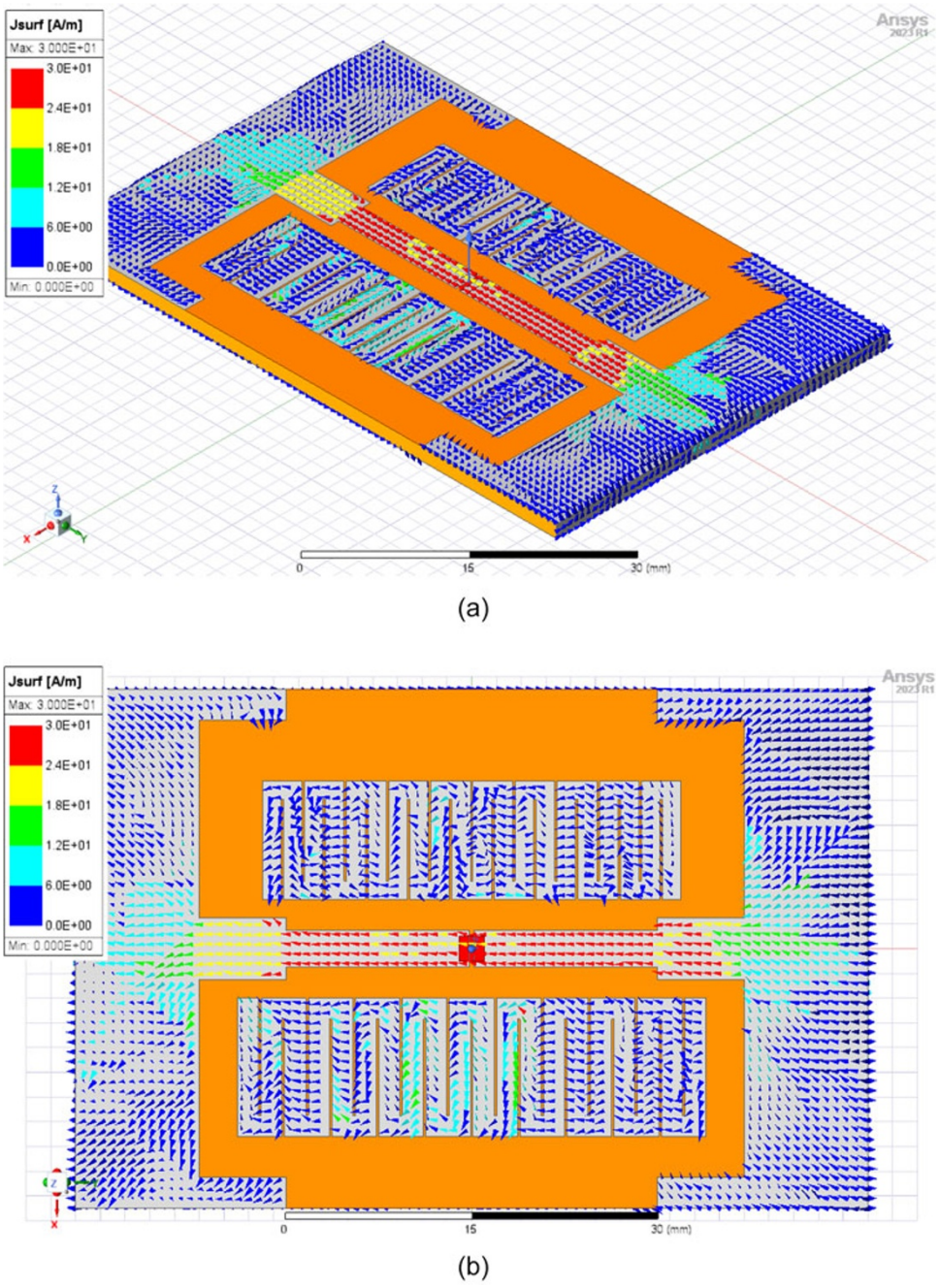


Figure 10. Surface current distribution of the dual-coupled patches. (a) Isometric view. (b) Top view.

was compact and low-cost. However, the narrow tuning range (±5 MHz around 915 MHz) limited its regional adaptability. The low-profile PIFA in [20] permitted post-fabrication tuning through a U-slot and lumped elements. Nevertheless, its read range was limited to 3.6 m, and the via-based shorting structure complicated the fabrication process, which reduced the production yield to below 85%. [21] presented a magnetically coupled dual-resonance patch antenna that achieved an 11.5 m read range without shorting elements. However, it was large in size, sensitive to gaps, and restricted to the NA band. The stacked PILA in [22] lowered the resonance frequency to 867 MHz via capacitive coupling, which resulted in a read range of 7.01–7.88 m. Yet, it required folding assembly and could only be tuned within a narrow band of 865–868 MHz. Finally, the zeroth-order serpentine antenna from [24] offered a planar omnidirectional radiation pattern, a read range of 8–9 m, and a low profile. However, it was bulky and its performance degraded by over 20% on uneven metal surfaces due to its double-layer stack structure.

To further clarify the relative strengths of the proposed design, the main advantages and limitations are summarized as follows:

Advantages:

- Stable on-metal performance ensured by the magnetic-dipole-dominated radiation mechanism.

https://doi.org/10.1017/S1759078726103249 Published online by Cambridge University Press

Table 2. Table of comparison between designed antenna and published work

Ref	Publication year	Tag size (mm^2)	Thickness (mm)	Shorting elements	Substrate	Read range (m)
[16]	2021	30×30	3.0	Shorting wall	FR4	6.4
[20]	2021	29.8×29.8	0.813	Vias	Rogers RO4003C	3.6
[21]	2021	118×42	1.6	None	Rogers 5880	11.5
[22]	2021	31.5×31.5	3.2	Stubs	Foam	7.2
[14]	2022	50×50	3.32	None	Foam	9.0
[8]	2024	56 (Dia)	1.5	None	PTFE	9.5
[10]	2024	39×39	1.38	None	6010LM-RT-Duroid	10.1
[15]	2024	40×30	1.65	Stubs	Rogers RO4003C	4.7
[24]	2024	50×50	3.38	Walls	Foam	8.5
This work	——	64×42	1.6	Stubs	FR4	7.32

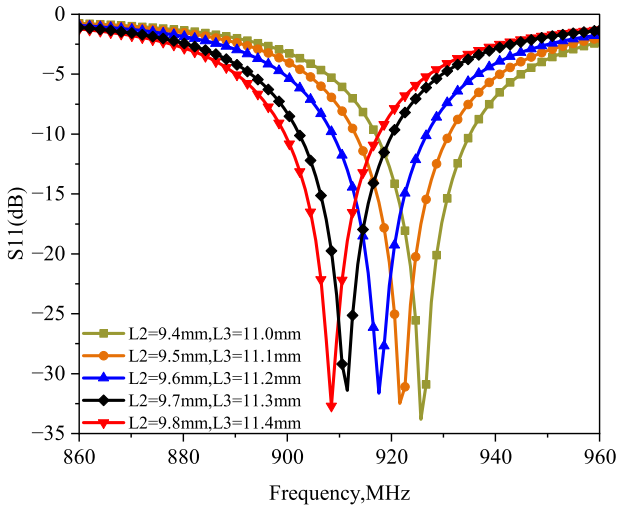


Figure 11. The center frequencies varying with *L*2,*L*3.

- Broadband impedance matching achieved through dual-resonant coupling.
- Simple fabrication without multilayer stacking or via-based shorting walls.
- Frequency controllability by tuning dipole lengths and coupling spacing.

Limitations:

- The achievable gain is constrained by the compact aperture.
- Performance may be affected by fabrication tolerance of the soldered shorting stubs.

In comparison, our tag design exhibits several distinct advantages. It adopts a simple single-substrate structure without folds or via interconnections, which enhances mechanical stability and reduces fabrication complexity. Unlike many existing designs that rely on material engineering or multilayer stacking, the proposed tag emphasizes structural-level mode and coupling engineering. This strategy enables wide frequency tuning without additional lumped elements, thereby improving cost-effectiveness. These results confirm its practicality for actual UHF RFID applications.

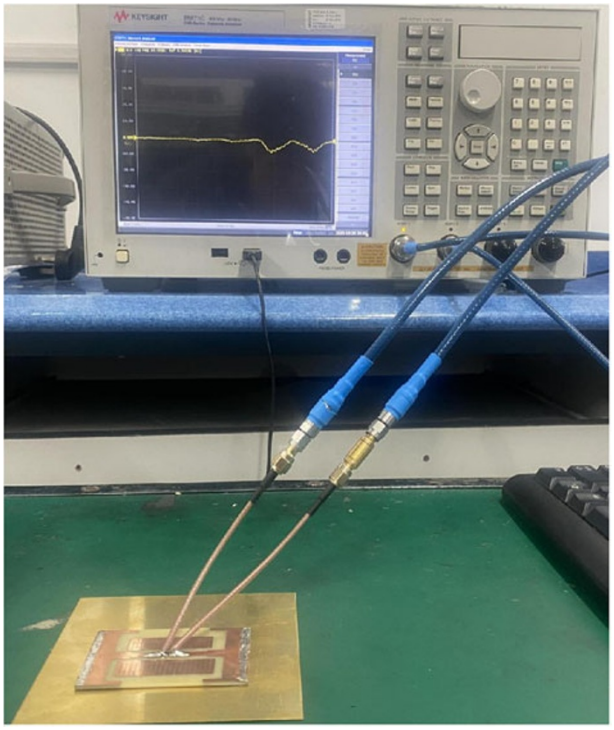


Figure 12. Actual impedance measurement of the tag by vector network analyzer.

Conclusion

A novel magnetic loop structure antenna is proposed for designing metal-mountable omnidirectional UHF RFID tags. Short wires are used to connect the feed line and the ground plane, which forms a vertical loop configuration that supports magnetic-dipole-dominated radiation. The portion of the antenna in contact with the metallic surface effectively isolates the radiating patch from the metal, thereby ensuring stable on-metal performance. Furthermore, asymmetric bent dipoles are electromagnetically coupled to the feed line to introduce an auxiliary electric resonance. This magnetic–electric mode interaction enables improved conjugate matching with the RFID microchip and enhanced operating bandwidth without increasing structural complexity. A prototype of the proposed tag antenna was fabricated and experimentally

https://doi.org/10.1017/S1759078726103249 Published online by Cambridge University Press

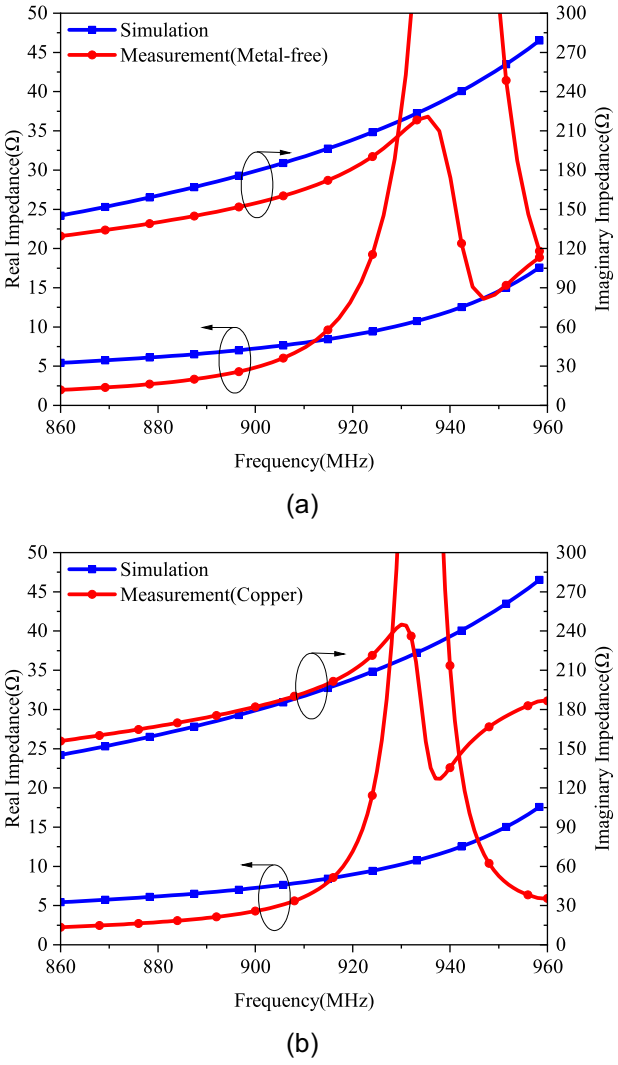


Figure 13. Measured and simulated impedance. (a) In free space. (b) On copper sheet.

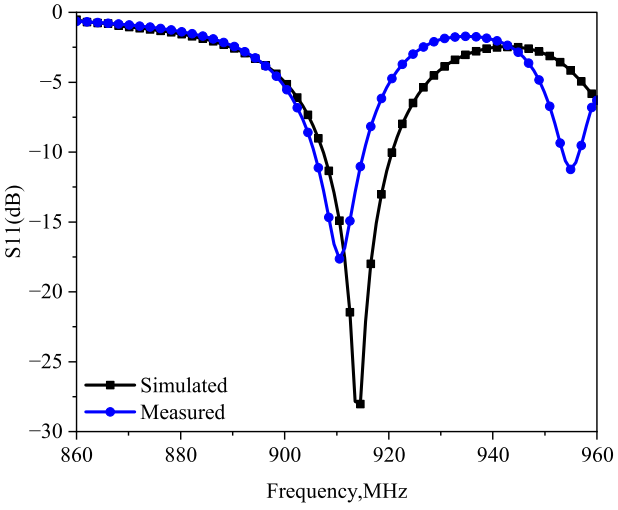


Figure 14. The simulation and measurement comparison of S11.

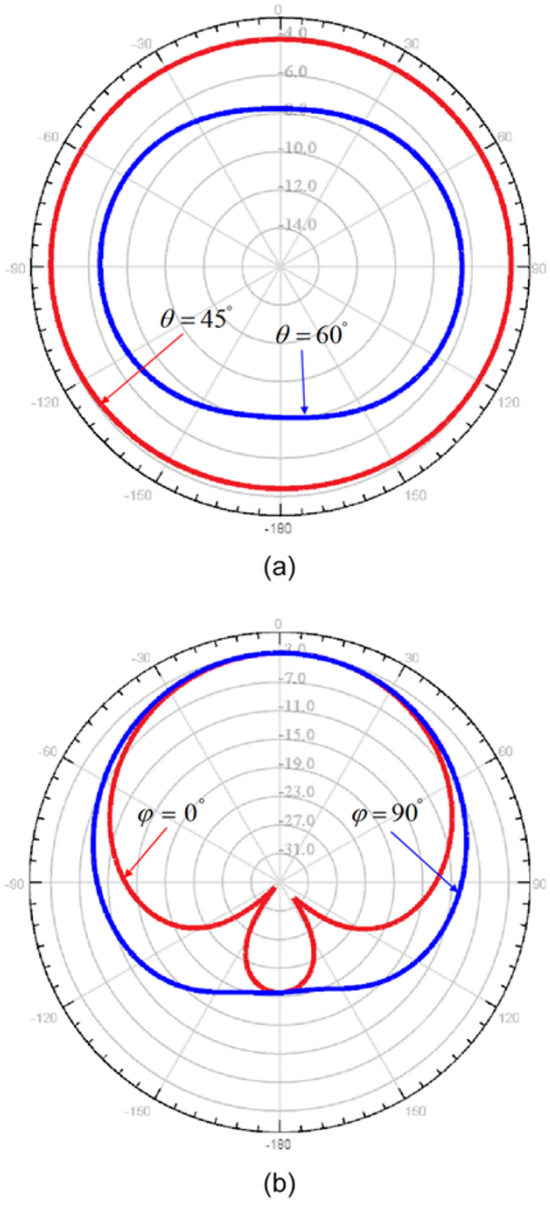


Figure 15. (a) XY plane read pattern. (b) XZ and YZ plane read pattern.

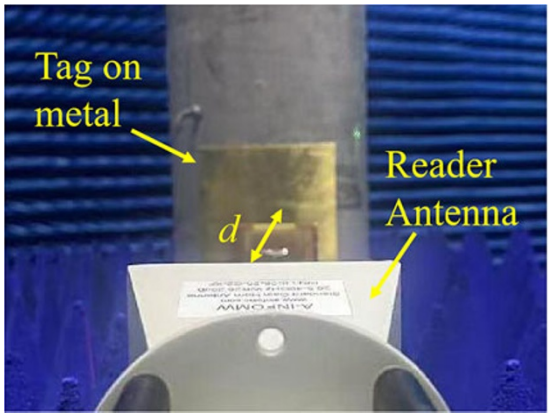


Figure 16. Measurement of the recognition distance in darkroom.

https://doi.org/10.1017/S1759078726103249 Published online by Cambridge University Press

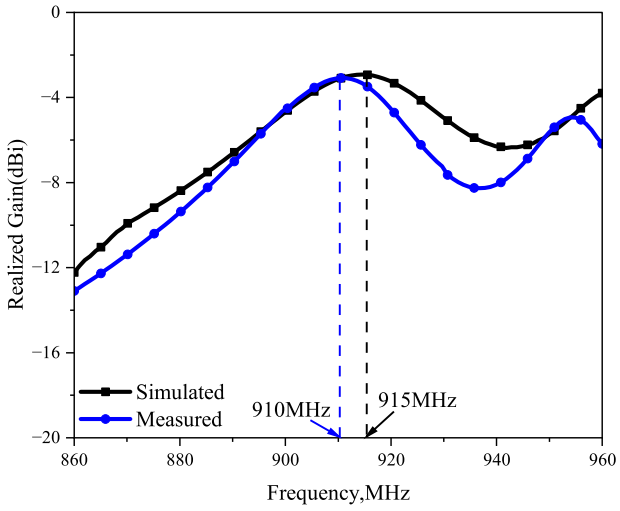


Figure 17. The measured and simulated gains of the antenna.

evaluated. The measured results demonstrate that the antenna maintains stable radiation characteristics on metal surfaces and achieves an effective read range of 7.32 m. This performance is obtained while maintaining a compact size and low-profile structure, which is well suited for practical UHF RFID tagging applications. The proposed design effectively addresses the challenge of reliable RFID detection in metallic environments and meets the size and performance requirements of applications such as logistics management.

Acknowledgements. This work was supported by the National Natural Science Foundation of China under Grant Nos. 62371245 and 62371248, Science and Technology Research and Development Program of China State Railway Group Co., Ltd (L2024G006), China Unicom Internet of Things Co., Ltd project (SZ93-0401-2025-000322), and The Science Foundation of Nanjing University of Posts and Telecommunications (XK0300922130).

Competing interests. The authors declare no potential conflict of interests.

References

1. **Li S, Xu LD and Zhao S** (2015) The internet of things: a survey[J].), 243–259.
2. **Finkenzeller K** (2010) *RFID Handbook: Fundamentals and Applications in Contactless Smart Cards, Radio Frequency Identification and Near–Field Communication[M].* John Wiley & Sons,.
3. **Abdulghafor R, Turaev S, Almohamedh H, Alabdan R, Almutairi B, Almutairi A and Almotairi S** (2021) Recent advances in passive UHF–RFID tag antenna design for improved read range in product packaging applications: A comprehensive review[J]. , 63611–63635.
4. **Marrocco G** (2008) The art of UHF RFID antenna design: Impedance–matching and size–reduction techniques[J].), 66–79.
5. **Balanis CA** (2016) *Antenna Theory: Analysis and Design[M].* John Wiley & Sons.
6. **Lee YH, Lim EH, Bong FL and Chung BK** (2018) Compact folded C–shaped antenna for metal–mountable UHF RFID applications[J].), 765–773.
7. **Bansal A, Sharma S and Khanna R** (2020) Platform tolerant dual–band UHF–RFID tag antenna with enhanced read range using artificial magnetic conductor structures[J].), e22065.
8. **Erman F, Koziel S, Lim EH, Leifsson L, Hanafi E and Murugesh M** (2024) A low–profile metal–backed dipole loaded with closely coupled arc–shaped open stubs for on–metal tag design with wide frequency tuning capability[J].), 3772–3777.
9. **Mathew T and BM Varghese** (2024). UHF RFID dipole tag with asymmetrically loaded trapezoidal spiral arms [C]//2024.. *IEEE 21st India Council International Conference (INDICON)*. IEEE, pp. 1–4.
10. **Murugesh M, Rahim SK, Lim EH and Chee PS** (2024) A low–profile patch–loaded ring antenna with wide frequency tuning capability for dual–band metal–mountable tag design[J]..
11. **Lee SR, Ng WH, Lim EH, Bong FL and Chung BK** (2019) Compact magnetic loop antenna for omnidirectional on–metal UHF tag design[J].), 765–772.
12. **Lee SR, Ng WH, Lim EH and Rahim SK** (2023) Loop–coupled small antenna with enhanced bandwidth for on–metal UHF RFID tag design[J].), 3660–3664.
13. **Murugesh M and Akbar MF** (2025) A low–profile symmetric dipole UHF RFID tag design with wide tuning range for metallic platforms. , 415–425.
14. **Murugesh M, Lim EH, Chee PS and Bong FL** (2022) Complementarily coupled C–shaped microstrip patches with wide–range frequency tuning capability for metal–applicable UHF RFID tag design[J].), 11548–11558.
15. **Ng GJ, Lim EH, Chee PS and Murugesh M** (2024) Design of dual–band UHF RFID tag antenna using even and odd modes of asymmetric split ring for anti–metal applications[J]..
16. **Nguyen MT, Lin YF, Chang CH, Chen CH and Chen HM** (2021) Compact shorted C–shaped patch antenna for ultrahigh frequency radio frequency identification tags mounted on a metallic plate[J]. *International Journal of RF and Microwave Computer–Aided Engineering* **31**(6), e22595.
17. **Nikitin P, M Brewster, J Kim and KV Rao** (2024). Magnetic sensing using T–Matched RAIN RFID Tags[C]//2024. *IEEE International Conference on RFID (RFID)*. IEEE, pp. 1–6.
18. **Sultan QH and Sabaawi AMA** (2021) Design and implementation of improved fractal loop antennas for passive UHF RFID tags based on expanding the enclosed area[J]. *Progress In Electromagnetics Research C* **111**, 135–145.
19. **Song C and Wu Z** (2022) A loop antenna array with an enlarged near–field interrogation zone for UHF RFID near–field and far–field applications[J]. *IEEE Antennas and Wireless Propagation Letters* **21**(10), 1985–1989.
20. **Inserra D and Wen G** (2021) Low profile metal tolerant UHF RFID tag with lumped elements for post–manufacturing frequency tuning[J]. *IEEE Transactions on Antennas and Propagation* **69**(11), 7953–7958.
21. **Aslam B, Kashif M, Amin Y and Tenhunen H** (2021) Low–profile magnetically coupled dual resonance patch antenna for UHF RFID applications[J]. *AEU–International Journal of Electronics and Communications* **133**, 153672.
22. **Ooi SY, Chee PS, Lim EH, Lee YH and Bong FL** (2021) Stacked planar inverted–L antenna with enhanced capacitance for compact tag design[J]. *IEEE Transactions on Antennas and Propagation* **70**(3), 1816–1823.
23. **Erman F, Koziel S, Hanafi E, Soboh R and Szczepanski S** (2022) Miniaturized metal–mountable U–shaped inductive–coupling–fed UHF RFID tag antenna with defected microstrip surface[J]. *IEEE Access* **10**, 47301–47308.
24. **Murugesh M, Lim EH, Chee PS and Bong FL** (2024) Zeroth–order serpentine antenna with omnidirectional radiation pattern for anti–metal tag antenna design[J]. *IEEE Journal of Radio Frequency Identification* **8**, 431–440.
25. **Murugesh M, Akbar MF and Ghazali NA** (2025) Compact dipolar patch UHF RFID tag antenna using interdigital capacitor for metal platforms[J]. *IEEE Access*.
26. **Lo CC and YS Chen** (2025). Miniature dual–band tag antennas via stacked integration of a folded dipole and Dual–Patch for Anti–Metal RFID[J]. *IEEE Antennas and Wireless Propagation Letters*.
27. **Nguyen MT, Lin YF, Chen CH, Luong HS and Chen HM** (2025) Low profile planar inverted–l antenna (PILA) for UHF RFID Tag on signal absorption and reflection surfaces[J]. *IEEE Access*.

https://doi.org/10.1017/S1759078726103249 Published online by Cambridge University Press



Xueliang Yang is currently pursuing a master's degree at Nanjing University of Posts and Telecommunications. His research interests include antennas and propagation.



Fei He received a bachelor's degree in aeronautical manufacturing engineering from Beijing University of Aeronautics and Astronautics, China, in 1997, the master's degree in information management from Nanjing University, China, in 2005, and is currently pursuing a Ph.D. in Electronic Information Engineering at Nanjing University of Posts and Telecommunications.



Peng Wang is currently pursuing a master's degree at Nanjing University of Posts and Telecommunications. His research interests include digital signal processing.



Kaichao Wang is currently pursuing a master's degree at Nanjing University of Posts and Telecommunications. His research interests include digital signal processing.



Yuanjian Liu received his Ph.D. degree in Electromagnetic Field and Microwave Technology from Nanjing University of Posts and Telecommunications in 2009. His main research interests include ray tracing methods and their engineering applications, indoor short-range wave propagation, and indoor and outdoor wireless network coverage for complex environments.



Zhenzhen Tu received her Ph.D. degree in Biochemistry and Molecular Biology from China Pharmaceutical University in 2012. Her main research interests include molecular diagnosis and targeted therapy of tumors, material science and engineering, nano probes and bioimaging technology, and information sensing and imaging technology.



Weigang Wang received his M.S. degree in Circuits and Systems from Nanjing University of Posts and Telecommunications in 2006 and the Ph.D. degree in Signal and Information Processing from Nanjing University of Posts and Telecommunications in 2015. His main research interests include wireless communication technology and signal processing.

https://doi.org/10.1017/S1759078726103249 Published online by Cambridge University Press